THE JOURNAL OF PHYSICAL CHEMISTRY C

Article

pubs.acs.org/JPCC

Lithium-Ion Model Behavior in an Ethylene Carbonate Electrolyte Using Molecular Dynamics

Narendra Kumar[†] and Jorge M. Seminario*[,†,‡,§]

[†]Department of Chemical Engineering, [‡]Department of Electrical and Computer Engineering, and [§]Department of Materials Science and Engineering, Texas A&M University, College Station, Texas 77843, United States

ABSTRACT: The performance of lithium-ion batteries is strongly dependent on the nature of the electrolyte, and a better understanding of the role of the electrolyte in ion transport and the formation of the solid−electrolyte interface is critical for the performance improvement of such batteries. New cathode and anode materials demand new and/or improved electrolytes that are less sensitive to operating conditions and provide higher conductivity and mobility of ions between electrodes. A clear understanding of the solvation of electrolytes in solvents is essential for improving the performance and cycle life of Li-ion batteries. In this work, the behavior of lithium hexafluorophosphate ($LiPF_6$) in ethylene carbonate was characterized using classical molecular dynamics simulations and ab initio density functional theory (DFT) calculations. The solvation structures of both Li^+ and PF_6^- in the electrolyte were analyzed in detail, and the intermolecular and intramolecular potentials were found to produce all of the essential features of the electrolyte as observed from ab initio DFT calculations. The thermodynamics and transport properties obtained using molecular dynamics simulations were also found to be in good agreement with experimental values.

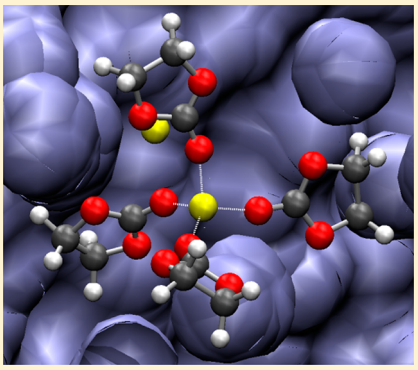

1. INTRODUCTION

The importance of developing new electrolytes with suitable solvents for modern batteries requires good knowledge of the chemistry and physics of the present electrolytes. The fact that a search for better and more powerful batteries is in progress triggered our curiosity in finding ways to design new materials involving the safer and more efficient use of alternative power sources away from fossil fuels.[1−12]

One of our goals in this work was to determine the ability of existing models for electrolytes based on molecular dynamics (MD) simulations to determine key characteristics of existing electrolytes and, thus, to predict the behavior of new electrolytes and solutions.[13−18] The use of classical atomistic models or force fields was chosen because of the possibility of obtaining parameters direclty from ab initio calculations without the need for an initial set of experimental information, allowing for trials to be performed *in silico*.

A large amount of work has been done and much progress has been made regarding the development of force fields and their use in molecular dynamics calculations for specific application to battery electrolyte solutions. Both polarizable and nonpolarizable force fields have been used to obtain structure and transport properties of ions and solvents in lithium-ion batteries. Soetens et al.[19] used a combination of 12−6 Lennard-Jones parameters from the optimized potential for liquid simulations (OPLS) all-atom (AA) force field[20] and atomic charges obtained by fitting the electrostatic potential calculated using Hartree−Fock calculations and the 6-31G** basis set. The bonded interactions were obtained from the CFF91 force field.[21] Molecular dynamics simulations performed for $Li^+BF_4^-$ solvated in ethylene carbonate (EC), propylene carbonate, and dimethyl carbonate revealed that lithium ions were solvated by the electrolytes in a tetrahedral coordination.[19] The BF_4^- ions were solvated by 19−20 solvent molecules in the first coordination shell; however, their coordination shell was dificult to distinguish. The same nonbonded interaction parameters along with modified AMBER parameters[22] for bonded interactions were later used by Masia et al.[23] to study the structure and vibrational properties of lithium ions solvated by EC. They also analyzed the structural properties and vibration spectra of a single EC molecule and $(EC)_n$−Li^+ clusters using Møller−Plesset perturbation theory.[23] The solubilities of several lithium salts in EC and dimethyl carbonate were studied using a simulation package using the COMPASS (Condensed-Phase Optimized Molecular Potentials for Atomistic Simulation Studies) force field with electrostatic potential (ESP) charges obtained with the Perdew−Burke−Ernzerhof (PBE) functional.[24] The van der Waal's parameters were directly obtained from the Accelerys automatic parameter generator Materials Studio.[25] In another work, Takenaka et al.[6] analyzed the microscopic characteristics of the solid−electrolyte interface layer formed by oxidation/reduction of the electrolyte on a graphite layer using a hybrid Monte Carlo/molecular dynamics simulation with the general AMBER force field (GAFF)[26] and partial atomic charges obtained using rescaled ESP charges calculated at the B3LYP/6-31+G(d) level. The force field parameters of Masia et al.[23] were further modified by applying a force-matching algorithm

Received: April 12, 2016
Revised: June 23, 2016
Published: July 8, 2016

DOI: 10.1021/acs.jpcc.6b03709
J. Phys. Chem. C 2016, 120, 16322−16332

to construct a new force field for the pure EC electrolyte as well as $LiPF_6$ dissolved in EC from ab initio molecular dynamics simulations.[27] The effects of the composition of the solid−electrolyte interface (SEI) layer and its thickness on ion transport in lithium-ion battery as a function of applied voltage were investigated using the newly developed force field.[27] On the other hand, classical many-body polarizable force fields were also developed for carbonate-based solvents that can reliably predict thermodynamic, structural, and transport properties.[28] The polarization effects were included using an atomic dipole polarization model.[28] Many-body polarizable force fields were also developed for PF_6^- ions and other ionic liquids.[29] Using these polarizable force fields, molecular dynamics simulations were performed on a mixture of EC and dimethyl carbonate containing $LiPF_6$ as a lithium salt near a graphene surface,[30] showing that the composition of the interfacial layer of the electrolyte near the graphite depends on the electrode potential.[30] The transport of lithium ions in diethyl carbonate was also studied using molecular dynamics simulations with a many-body polarizable force field.[31] A reactive force field (ReaxFF) was also developed to investigate reactions involving EC.[32] Recently, the solvation structures of lithium and PF_6^- ions in ethylene carbonate, ethyl methyl carbonate, and their binary mixture were analyzed using first-principles molecular dynamics and the ReaxFF.[33] Some of the $LiPF_6$ molecules remained in associated form throughout the simulations, whereas others underwent dissocation; the coordination number for associated ion pairs was ∼2.5, whereas in the case of dissociated ion pairs, the coordination number around Li^+ ions was 4. PF_6^- ions were weakly solvated with poorly structured solvation shells and very short molecular residence times. The diffusion coefficient of Li^+ was found to be lower than that of PF_6^- ions, and higher diffusion coefficients were obtained in the case of ethyl methyl carbonate than ethylene carbonate.[33]

2. METHODOLOGY

The quantum chemical calculations in this work were performed using Gaussian 09 program[34] with the B3PW91 functional[35−39] and the 6-311++G(d,p) basis set[40,41] for all atoms. Geometry optimizations are followed by second-derivative calculations to ensure that a local minimum was reached in all cases.

All of the molecular dynamics (MD) simulations were performed using the Large-Scale Atomic/Molecular Massively Parallel Simulator (LAMMPS) program.[42] This program has been used successfully in several applications related to nanotechnology.[43−48] The simulation box contained 675 EC molecules, 45 Li^+ ions, and 45 PF_6^- ions distributed randomly, corresponding to a 1 M concentration of $LiPF_6$ salt in EC. The box size initially chosen was 66.1 × 33.9 × 33.9 $Å^3$, corresponding to a density of 1.3 g/cm^3 of pure EC, which changed to 1.45 g/cm^3 when the salt was added. The initial atomic coordinate file was generated with the Packing Optimization for Molecular Dynamics Simulations (Packmol) program.[49] Periodic boundary conditions (PBCs) were applied in all three directions, and the system was first equilibrated at 5 K and then heated to 330 K in the *NPT* ensemble to allow for a change in volume due to the addition of $LiPF_6$ to the electrolyte. A cutoff of 12 Å was used for van der Waals (vdW) interactions, and a long-range correction [particle−particle particle-mesh (pppm)] was used for Coulombic interactions with a cutoff of 12 Å. The nonbonded interaction parameters and charges for EC were taken from Masia et al.,[23] whereas those for PF_6^- were taken from Jorn et al.,[27] except for the Lennard-Jones (LJ) parameter σ for phosphorus, which was taken from the universal force field (UFF).[50,51] After being heated to 330 K, the simulation box was equilibrated at 330 K for 3 ns with a time step of 1 fs in the *NVT* ensemble, and then a production run was conducted for another 5 ns for equilibration and parameter calculations. We also ran dynamics by heating the system from 5 to 800 K in the *NPT* ensemble to observe the thermodynamic phase behavior of EC. Visualization of the trajectories was performed using the graphics software package Visual Molecular Dynamics (VMD).[52]

Bonded interactions such as bond stretching, angle bending, torsion, and improper dihedrals for EC were taken from a class II force field,[21] as it produced the correct nonplanar geometry of EC. It has been already mentioned in the literature that class II force fields such as CFF91 and CFF93[21] yield structures in agreement with the minimum-energy structures of EC, PC, and DMC. On the other hand, barriers to conformational inversion yielded by class II force fields are also comparable to those from other nonpolarizable force fields such as AMBER[22] and CVFF[53] commonly used to model organic compounds.[19] Consequently, the CFF93 force field was chosen to describe the intramolecular interactions of the three carbonate molecules. Although class II force fields have been shown to perform better for carbonates and polymers,[27] they use a 9−6 Lennard-Jones potential that gives a stronger attraction at longer distances. A 12−6 Lennard-Jones potential, on the other hand, gives a stronger repulsion at closer distances.[54] However, the effect of this choice was not that critical for the properties of interest.[54] For our study, we used a 12−6 Lennard-Jones potential, the parameters of which are listed in Table 1. Harmonic-style bond-stretching (K_b = 370.8 kcal/mol and b_0 = 1.606 Å) and angle-bending (K_θ = 139.4 and θ_0 = 90°) potentials were used for the PF_6^- anion.[55]

Table 1. Nonbonded LJ Parameters and Partial Atomic Charges Used for the Simulation of 1 M $LiPF_6$ Solvated in EC

atom/pair type[a]	ε (kcal/mol)	σ (Å)	q (e)
O_x	0.210	2.96	−0.6452
C_x	0.105	3.75	1.0996
O_s	0.170	3.00	−0.4684
C	0.066	3.50	0.0330
H	0.030	2.50	0.1041
Li	0.10314	1.4424	1.0
P	0.13169	3.695	1.07
F	0.028716	2.9347	−0.345
Li−O_x	0.05551	2.398	
Li−P	0.014033	3.007	
Li−O_s	0.20937	2.0217	
F−H	0.2056	2.3951	
F−C_x	0.06546	2.9381	

[a]O_x and C_x are the carbonyl oxygen and carbon, respectively; O_s represents the ether oxygens; C represents the carbons in EC.

The dynamic properties of lithium ions in electrolyte solution were characterized in terms of both the diffusion coefficient and the ionic mobility. The diffusion coefficient was obtained from the slope of a plot of the mean-square displacement versus time using the Einstein equation following a long equilibration of the simulation box. The ionic mobility

DOI: 10.1021/acs.jpcc.6b03709
J. Phys. Chem. C 2016, 120, 16322−16332

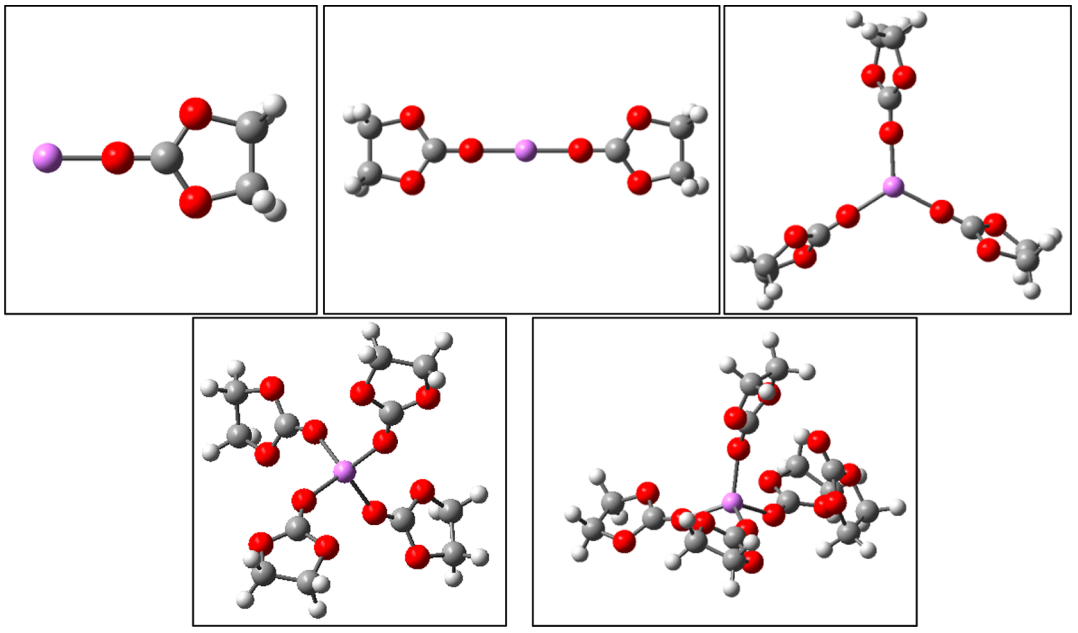

Figure 1. Optimized structures of $(EC)_nLi^+$ (n = 1, 2, 3, 4, 5) clusters at the B3PW91/6-311++G(d,p) level of theory.

Table 2. Total (E) and Binding (D) Energies, Li−O_x Distances from the Li Ion to the O Atom of the Carbonyl Group in EC, and Mulliken and Natural Populations of $(EC)_nLi^+$ Clusters at the B3PW91/6-311++G(d,p) Level of Theory

				Mulliken		natural	
complex	E (hartree)	D (kcal/mol)	Li−O_x (Å)	q_{Li}	q_{O_x}	q_{Li}	q_{O_x}
Li^+	−7.27961			+1.0		+1.0	
EC	−342.36903				−0.33		−0.56
EC−Li^+	−349.72757	−49.5	1.75	+0.80	−0.36	+0.97	−0.81
$(EC)_2$−Li^+	−692.15622	−86.9	1.80	+0.07	−0.18	+0.90	−0.74
$(EC)_3$−Li^+	−1034.56035	−109.0	1.87	+0.47	−0.28	+0.81	−0.67
$(EC)_4$−Li^+	−1376.95079	−122.4	1.96	−0.05	−0.16	+0.71	−0.62
$(EC)_5$−Li^+	−1719.33098	−129.4	1.96	−0.04	−0.10, −0.29[a]	+0.70	−0.62, −0.65[a]

[a]Inner shell contains only four EC molecules and the fifth forms a second shell.

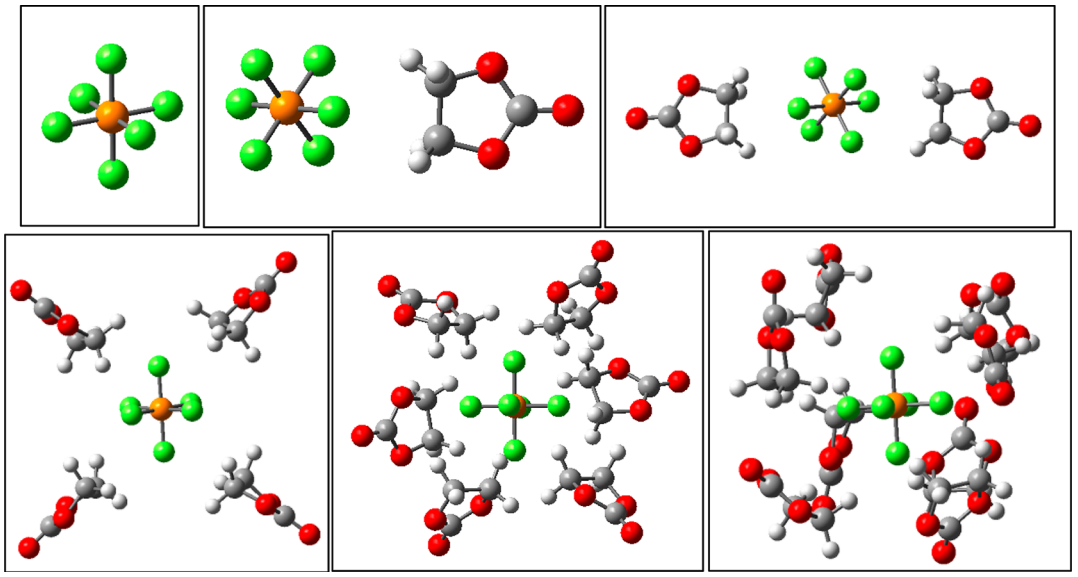

Figure 2. Optimized structures of $(EC)_nPF_6^-$ (n = 0, 1, 2, 4, 6, 8) clusters at the B3PW91/6-311++G(d,p) level of theory.

was calculated from the average drift velocity of lithium ions under a unidirectional external field. We followed a procedure similar to that of Shi and co-workers,[56,57] who showed that the drift velocity could be obtained from a finite trajectory by

DOI: 10.1021/acs.jpcc.6b03709
J. Phys. Chem. C 2016, 120, 16322−16332

Table 3. Total (E) and Binding (D) Energies, P−O_x Lengths, and Mulliken and Natural Populations of $(EC)_nPF_6^-$ (n = 0, 1, 2, 4, 6, 8) Clusters at the B3PW91/6-311++G(d,p) Level of Theory

				Mulliken			natural		
molecule	E (hartree)	D (kcal/mol)	P−O_x (Å)	q_P	q_F	q_H	q_P	q_F	q_H
PF_6^-	−940.61642			+0.52	−0.25		+2.53	−0.59	
$(EC)-PF_6^-$	−1283.00781	−14.0	7.23	+0.42	−0.23	+0.26	+2.53	−0.59	+0.21
$(EC)_2-PF_6^-$	−1625.39611	−26.1	7.28	+0.17	−0.18	+0.26	+2.53	−0.59	+0.21
$(EC)_4-PF_6^-$	−2310.16113	−43.0	7.43	−0.39	−0.10	+0.27	+2.53	−0.59	+0.20
$(EC)_6-PF_6^-$	−2994.91533	−53.2	7.56	−1.21	−0.01	+0.27	+2.53	−0.58	+0.20
$(EC)_8-PF_6^-$	−3679.68254	−71.5	6.10	−1.72	+0.11	+0.24	+2.53	−0.58	+0.21

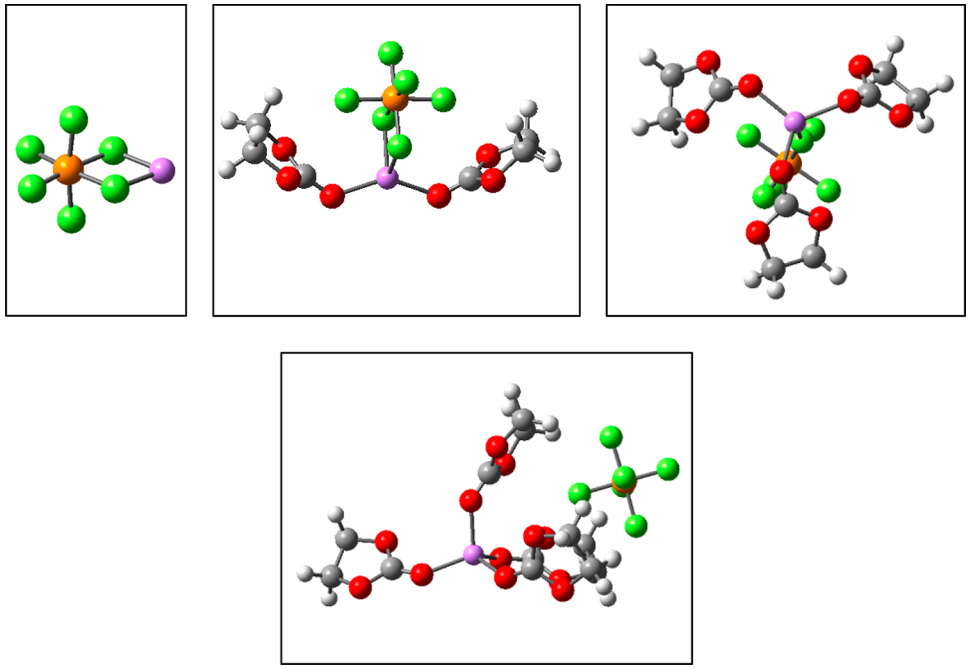

Figure 3. Optimized structures of $(EC)_nLiPF_6$ (n = 0, 2, 3, 4) clusters at the B3PW91/6-311++G(d,p) level of theory.

averaging the displacement in the direction of the applied field over time. Here, we estimated the drift velocity of each lithium ion by dividing the total displacement in the direction of the applied field by the simulation time, accounting for the periodic boundary conditions. Then, we used the drift velocity averaged over all lithium ions to obtain the ionic mobility using the equation $\mu = \langle V_d \rangle / E$, where μ is the mobility and E is the applied external electric field.

3. RESULTS AND DISCUSSION

The optimized structures of a lithium ion solvated by one to five EC molecules calculated using ab initio density functional theory (DFT) calculations are shown in Figure 1. The results show (Table 2) that the first solvation shell around the Li^+ ion can contain only up to four solvent (EC) molecules with an average Li−O_c distance of 1.96 Å, where O_c is the carbonate oxygen; any additional EC molecule enters the second solvation shell. The solvent molecules are coordinated in a tetrahedral fashion to the central ion. No consistent trend was observed from the Mulliken population analysis; however, the Mulliken population on lithium decreased in the presence of EC, and it was close to zero when Li^+ was coordinated to four EC molecules. It has already been pointed out in the literature that Mulliken populations for Li-containing compounds are highly variable and sometimes lead to populations opposite in sign to those expected from the difference in electronegativities.[58] Therefore, we also performed natural population analysis on these molecules, as such analyses are numerically more stable with respect to basis set changes and are able to better represent the electronic charge distributions in ionic compounds and molecules containing metals.[59] Unlike Mulliken population analysis, which divides the orbital overlap evenly between the two atoms involved, natural population analysis is based on occupancies of orthonormal natural atomic orbitals on each atomic center.[59] Natural population analysis showed that, as the number of EC molecules in the inner shell increased, the natural population of Li^+ and carbonyl oxygen decreased and remained unchanged when the fifth EC molecule was added.

Similarly, we obtained the solvated structures of a negative PF_6^- ion in EC (Figure 2, Table 3). The maximum coordination number of EC around PF_6^- ions was found to be eight, validating the average value calculated from the molecular dynamics simulation. The Mulliken population on fluorine atoms decreased and became positive as the number of EC molecules increased, whereas the populations on the hydrogen atoms of EC remained more or less unchanged. The decreases in negative population on fluorine atoms were compensated by a decrease in the positive population of the phosphorus atom. Unlike the Mulliken populations, the natural populations on the atoms remained unchanged, even when EC

DOI: 10.1021/acs.jpcc.6b03709
J. Phys. Chem. C 2016, 120, 16322−16332

Table 4. Total (E) and Binding (D) Energies and Mulliken and Natural (in Parentheses) Populations of $(EC)_nLiPF_6$ (n = 0, 1, 2, 3, 4) Clusters at the B3PW91/6-311++G(d,p) Level of Theory

cluster	E (hartree)	D	Li−O_x (Å)	Li−F (Å)	q_{Li}	q_{O_x}	q_P	q_F[b]
$LiPF_6$	−948.10594			1.79	+0.69 (+0.94)		+0.38 (+2.53)	−0.07, −0.23 (−0.55, −0.64)
$(EC)-LiPF_6$	−1290.51286	−23.8	1.86	1.84	+0.33 (+0.85)	−0.27 (−0.67)	+0.38 (+2.53)	−0.08, −0.20 (−0.55, −0.61)
$(EC)_2-LiPF_6$	−1632.91028	−41.6	1.92	1.98	−0.04 (+0.76)	−0.10 (−0.65)	+0.20 (+2.53)	−0.07, −0.16 (−0.56, −0.58)
$(EC)_3-LiPF_6$	−1975.29555	−51.8	1.96	1.99	+0.07 (+0.73)	−0.10 (−0.64)	+0.09 (+2.54)	−0.05, −0.14 (−0.57, −0.58)
$(EC)_4-LiPF_6$	−2317.67666	−59.4	1.97	4.34	+0.08 (+0.70)	−0.13, −0.18[a] (−0.64, −0.6[a])	+0.08 (+2.53)	−0.06, −0.18 (−0.58, −0.60)

[a]Inner shell contains only three EC molecules, and the fourth constitutes the second shell. [b]Smaller negative electron populations correspond to fluorine atoms closest to lithium ion.

molecules were present around the anion showing van der Waals type interactions between PF_6^- and EC.

In the case of the pure $LiPF_6$ complex (Figure 3, Table 4), the lithium ion is bonded to two fluorides from the PF_6^- in a bidentate mode. When solvent EC molecules were present, up to three EC molecules and one of the fluorine atoms from the PF_6^- anion surrounded the lithium ion, thus making a 4-coordinated structure for this case of an associated ion pair. Although the binding energy of the lithium ion to EC is weaker than that to PF_6^- ion, the lithium ion was bonded to PF_6^- in a monodentate fashion in the presence of the solvent. As a result, $LiPF_6$ can easily dissociate if any additional EC molecules are present in the vicinity of the $(EC)_3LiPF_6$ complex.

From the Mulliken population analysis, we observed that the positive populations on phosphorus and lithium atoms decreased whereas the negative populations on the fluorine atoms increased as the number of EC molecules increased. The negative population on the carbonyl oxygen atoms also decreased in the process. On the other hand, natural population analysis showed a different behavior. The positive population on lithium decreased when the number of EC molecules increased. However, the populations on the carbonyl oxygen, phosphorus, and fluorine atoms remained unchanged. It should be noted that Mulliken populations are strongly basis-set-dependent and can change radically when different basis sets are used. Therefore, individual charges cannot be used to draw conclusions here; however, to be consistent with earlier works that used Mulliken charges very frequently and very successfully, it is important to clarify that the issues with the Mulliken populations are simply because atomic charges do not correspond to any expectation value. Electron populations are lump factors representing the Coulombic behavior of a molecule in very simple terms. In this sense, populations should not necessarily be transferable. A value calculated for a specific type of atom in a molecule cannot be transferred to another molecule. Moreover, there are several ways to distribute the charge populations among the atoms in a given molecule. Thus, the known fact that different Mulliken populations can be obtained using different basis sets is not an issue as long as the complete set of charges for a given set are used.

We provide here a numerical demonstration (Figure 4) of this fact by calculating the electrostatic potential around a ring of 4-Å radius around a molecule of ethylene carbonate. We compare in Figure 4a the curves obtained using the natural bond orbital (NBO) populations with the cc-pVTZ basis set and the Mulliken populations with the 6-31G(d) and the cc-pVTZ basis sets (NBO/TZ, Mull/DZ, and Mull/TZ, respectively, in Figure 4a) with the exact curve obtained by solving the Schrodinger equation with the cc-pVTZ basis set. In all cases, the B3PW91 functional was used.

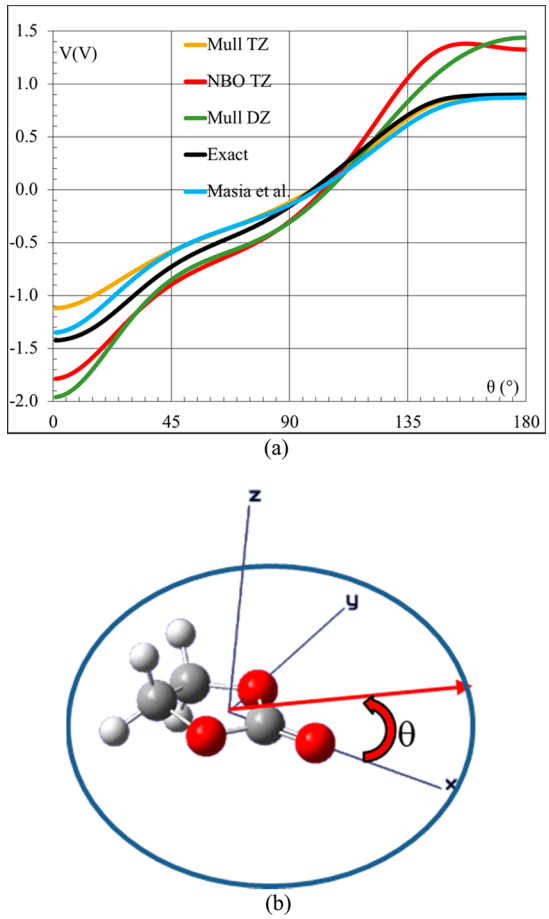

Figure 4. (a) Comparison of the exact potential versus the potentials obtained using NBO and Mulliken populations on the (b) 4-Å-radius blue circle around the EC molecule. The results obtained using the charges of Masia et al.[23] are also included. The "exact" potential was calculated at the B3PW91/cc-pVTZ level of theory.

Comparing first the Mulliken and NBO populations, one can notice (Figure 4a) that the Mulliken population analysis with the TZ basis set yields the best fit to the exact curve. On the other hand, Mulliken analysis with the DZ basis set and NBO analysis with the TZ basis set yield very similar results but not

DOI: 10.1021/acs.jpcc.6b03709
J. Phys. Chem. C 2016, 120, 16322−16332

as good as Mulliken analysis with the TZ basis set. Thus, what one can conclude from this isolated example is that abandoning the use of Mulliken populations simply because they yield several possible combinations of "charges" to represent the Columbic interactions of a molecule is a mistake. As long as populations are systematically calculated for all atoms in a molecule, it does not matter much whether one uses Mulliken or NBO charges. Interestingly, in this particular case of EC, better results are obtained for Mulliken than for NBO populations. We also included in Figure 4a the curve obtained with the set of parameters reported by Masia et al.[23] that we used extensively in this work. It yields a very good fit in this case, as its parameters were actually fitted to reproduce the electrostatic potentials, for which any of the others shown in Figure 4 were not, partially explaining the small divergences near 0° where the carbonyl oxygen is the closest atom to the ring (slightly less than 2 Å, entering into the bonded domain). In summary, we did not find any major quantitative or qualitative differences using any of the complete sets of electronic populations.

Next, we describe the results of MD simulations performed on 1 M $LiPF_6$ salt in EC. The simulation box was first equilibrated at 5 K in the *NPT* ensemble to relax the system. The volume immediately jumped from 76 to 89.4 nm^3 due to the presence of the lithium salt solvated in EC. Figure 5a shows the results of heating from 5 to 800 K, where one can observe three distinct zones. Although the melting point is difficult to discern from the volume−temperature plot because of the small difference in density between the solid and liquid phases, we analyzed the root-mean-square displacement (RMSD) of EC molecules over time as the temperature was increased from 5 K (Figure 5b). We observed a small increase in slope in the RMSD versus temperature plot near 280 K, which means that the EC molecules were more mobile at this point, indicating a change of phase from solid to liquid. The volume increased linearly to 100.7 nm^3 at 330 K, where EC was primarily in liquid phase. On further heating, the volume of the simulation box then increased exponentially after 530 K, indicating the onset of boiling. As a reference, the boiling point of pure EC is 521 K.[60]

To clarify further, we added colored arrows following the direction of the slope at a few points in Figure 5b, which helps demonstrate that the major change in slope takes place at 280 K (thickest red arrow). Certainly, the exception is for the change at ~5 K, which is simply due to the rearrangement of all ions and molecules in the system after the initiation of the simulations from a random generated distribution of solvent molecules and ions. We understand that this determination of the melting point by the slope of the RMSD versus temperature is not the best; however, because the RMSD values were obtained using the initial structure as a reference at 5 K, by visual inspection of trajectories during heating of the simulation box from 5 to 400 K, we observed that the molecules simply vibrated about their initial positions up to the temperature of 280 K. Thus, heuristically speaking, above 280 K, we observed an exchange of positions for different molecules. Thus, all events below 280 K in the slopes of the RMSD versus temperature plot are due to the relaxation of the simulation box and to molecular vibrations only. Figure 6 shows the last 5 ns of the 8 ns of equilibration at 330 K.

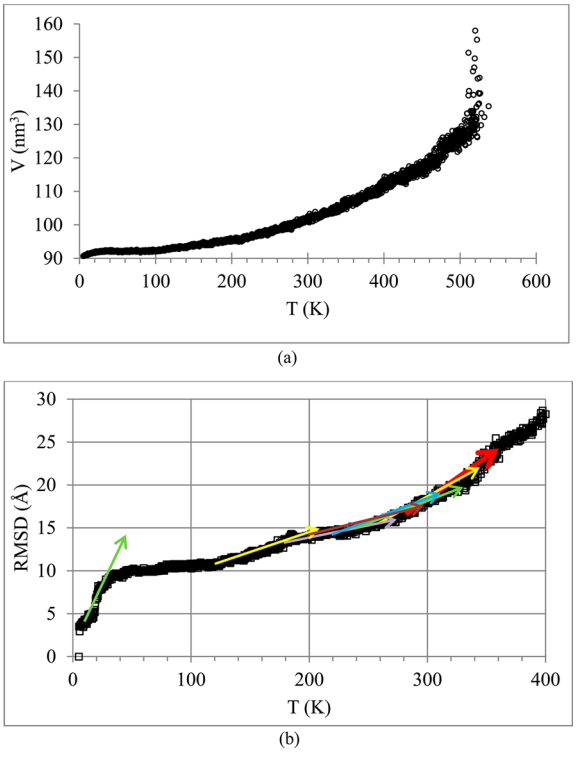

Figure 5. Heating of the 1 M $LiPF_6$ salt in EC mixture box in the *NPT* ensemble from 5 to 600 K: (a) volume (V) vs temperature (T) and (b) root-mean-square displacement (RMSD) vs temperature (T). Colored arrows are guides to follow the slope of the curve at several points approaching the melting point.

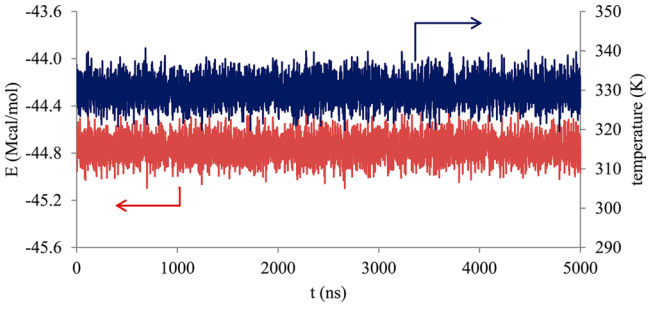

Figure 6. Temperature (T) and total energy (E) versus time (t) for the 1 M $LiPF_6$/EC mixture in the last 5 ns of equilibration at 330 K. The total equilibration time was 8 ns. Variations of energy around the average value of −44.8 Mcal/mol are on the order of only 1%.

Following equilibration for 8 ns at the expected operating temperature of ~330 K of the electrolyte solution, plots of the radial distribution functions (RDFs) for several noncovalently bonded atom pairs were obtained (Figure 7). The Li−O_c distribution plot (Figure 7a) shows the first peak at about 1.95 Å, which is in close agreement with Li−O_c distance calculated using density functional calculations for $(EC)_nLi^+$ clusters, n = 4, 5.

The nearest-neighbor distances of atomic pairs obtained from thermal equilibration at 330 K are listed in Table 5. These distances are compared with the bond lengths obtained using density functional theory calculations wherever available, as well as with the Lennard-Jones interaction parameter (σ).

The Li−O_c peak is predominantly determined by Coulombic interactions, as the positive contribution to the potential energy due to LJ interactions is 1/19th of the Coulombic interaction

DOI: 10.1021/acs.jpcc.6b03709
J. Phys. Chem. C 2016, 120, 16322−16332

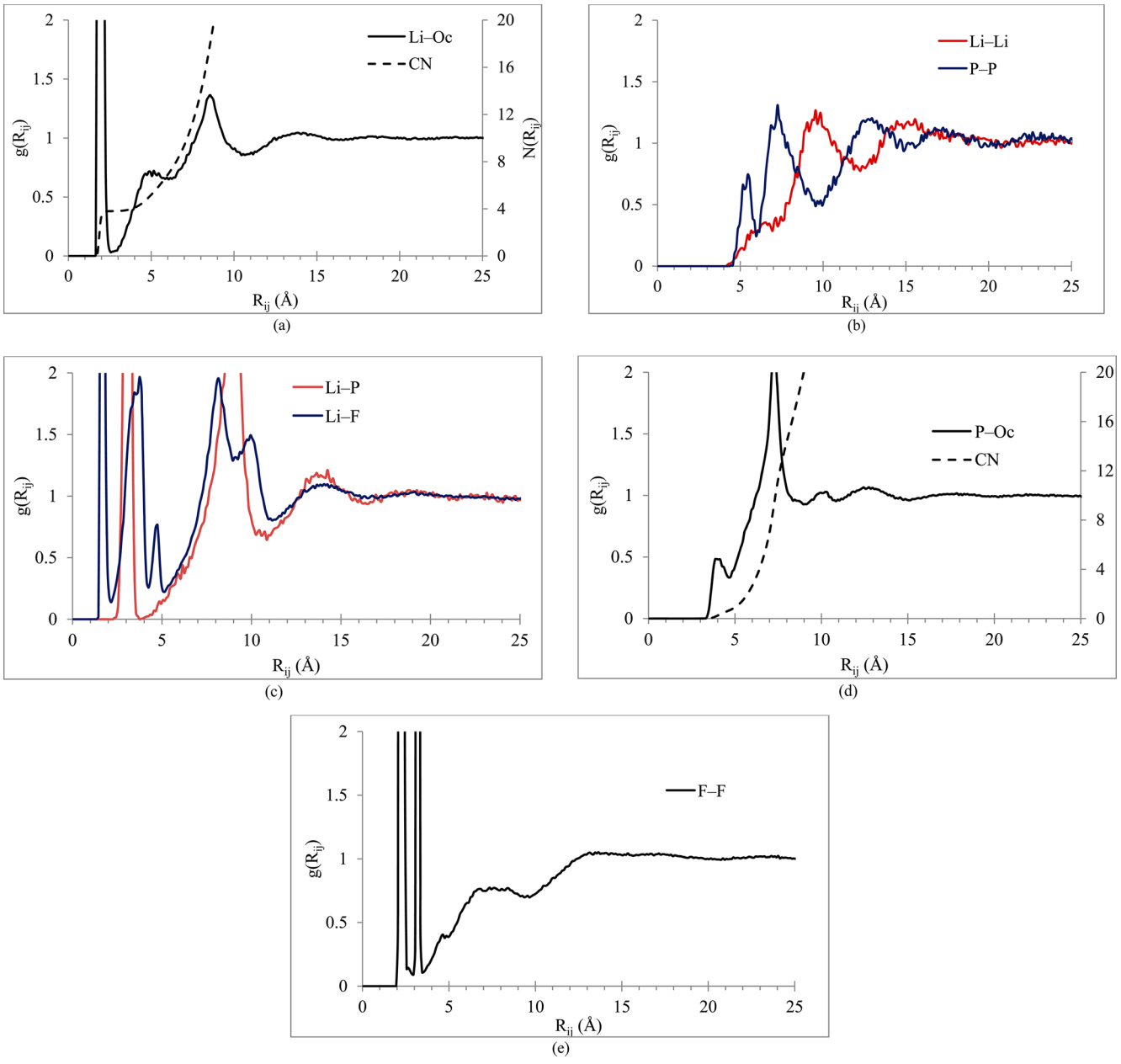

Figure 7. Radial distribution plots calculated after equilibration at 330 K for (a) Li^+ and carbonate oxygen (O_c) pair, (b) Li^+ dimer and P−P of PF_6^- dimer, (c) Li−P and Li−F pairs, (e) P of PF_6^- and carbonate oxygen, and (e) F−F of PF_6^- dimer.

Table 5. Comparison of Nearest-Neighbor Distances (NN), Bond Lengths (BL), and LJ Distance Parameters (σ) for the Important Ion-Pair Interactions in the MD Simulations

ion pair	NN (Å)	BL (Å)	σ (Å)
Li−O_c	1.95	1.96	2.398
Li−Li	6.35		1.4424
Li−P	3.15	3.60	3.007
P−P	5.35		3.695
F−F	2.25		2.9347
Li−F	1.65	1.99	2.057

energy at the minimum (1.85 Å) of the potential energy plot of EC−Li^+ pair. Similarly, the interaction between the PF_6^- and Li^+ ion pair is dominated by Coulombic interactions, with a minimum located at Li−P = 2.48 Å on the potential energy plot of the PF_6^- and Li^+ ion pair. The Li−Li, O_c−Li, Li−P, O_s−Li, H−F, and C_c−F LJ parameters were fitted by matching the forces between the force field and ab initio results for the EC−PF_6^-, EC−Li^+, and Li^+−PF_6^- pairs, and therefore, they depend on the atomic charges. For Li−Li, the peaks in the radial distribution functions are hardly distinguishable, with a first broad peak located at about 6.35 Å and a second wide peak located at 9.55 Å. The wider peaks present in the Li−Li RDF are due to the purely repulsive nature of the pair interaction. The first peak in the Li−P distribution function plot is located at 3.15 Å, which corresponds to the associated Li−PF_6 ion pair, whereas the broad second peak located at 8.95 Å corresponds to dissociated ion pairs. To determine the degree of association/dissociation of positive and negative ions, we analyzed the number of associated ion pairs formed over the trajectories during equilibration, where associated pairs are defined by a distance of Li−P < 4 Å using the information from

DOI: 10.1021/acs.jpcc.6b03709
J. Phys. Chem. C 2016, 120, 16322−16332

the Li−P pair distribution function plot. The time-averaged fraction of associated ion pairs during equilibration varies within the range of (18.3 ± 3.6)%. Consequently, the degree of ion dissociation in EC varies in the range of (81.7 ± 3.6)% at 330 K. For reference, the degree of dissociation measured experimentally using ion conductivity measurements was 71% at 303 K.[61] Comparing the Li−P radial distribution plot with the Li−O_c pair distribution plot, we conclude that two to three PF_6^- ions are present along with EC molecules in the second coordination shell around the Li^+ cation. The first two sharp peaks located at 2.25 and 3.25 Å in the F−F radial distribution function correspond to other fluorine atoms present in the same PF_6^- ion. The next peaks in the F−F radial distribution plot are broad and not well demarcated, indicating that the PF_6^- ions are weakly solvated and mobile in solvent. The Li−F radial distribution function is shown in Figure 7c. It is interesting to note that the first peak is located at 1.65 Å. Compared to the Li−F bond distance obtained for the 4-coordinated $(EC)_3LiPF_6$ cluster using ab initio density functional theory is 1.99 Å (Table 4). The P−O_c radial distribution function shows a small first peak at 3.95 Å that is close to the P−O_c distance obtained using quantum chemical calculations (4.34 Å) for the case when PF_6^- is present in the first coordination shell of the Li^+ ion. The second peak of P−O_c is located at approximately 7.25 Å, which is closer to the P−O_c distance calculated for $(EC)_nPF_6^-$ clusters at the B3PW91 level of theory.

The diffusion coefficient of lithium ions in EC was calculated using Einstein's equation. Figure 8 shows the mean-square displacement of lithium ions with the progress of simulation time. The 1/6 slope of the mean-square displacement versus time plot yields the value of the diffusion coefficient. We chose a linear region in the plot between 1.5 to 2.5 ns to calculate the diffusion coefficient. The diffusion coefficient of lithium ions in EC was calculated to be 1.44×10^{-10} m^2/s, which is close to the values reported by other researchers,[6,27,33,62] as well as to those from experiments.[61]

The ion mobility is another important dynamic quantity for examining the transport of ions through the bulk electrolyte and can be obtained from the drift velocities under an external electric field. Using the average value of the drift velocity, the mobility of Li^+ ion was calculated and is plotted against the applied field in Figure 9. The drift velocity increases linearly for small electric fields up to 0.2 V/Å and then increases exponentially as the field strength is further increased. The observed trend in drift velocity can be explained by observing the trajectories of lithium ions under the influence of an electric field. Below 0.2 V/Å, some of the Li^+ ions are trapped by PF_6^- ions during the motion and then behave as coupled ion pairs. When the applied field is sufficient to break the pair interaction between positive and negative ions, Li^+ ions start moving "freely", and therefore, there is an increase in drift velocity and, thus, in mobility. The calculated ion mobility can be compared with experimentally measured values. The mobility of Li^+ ions has been reported experimentally to be 3.6×10^{-9} $m^2/V{\cdot}s$ below 30 V in a lithium-gel electrolyte[63] and 7.2×10^{-9} $m^2/V{\cdot}s$ in an EC−diethyl carbonate mixture at about 15 V.[64] Experimentally, the ionic mobilities were obtained by diffusion measurements using a pulsed-gradient spin−echo NMR spectrometer under a constant electric field directly applied to the NMR sample and an electrophoretic technique for ion drifting.[63,64] A 15-V voltage for our simulation box of length 73.35 Å corresponds to ∼0.2 V/Å, yielding a mobility of 5.4×10^{-9} $m^2/V{\cdot}s$, which is consistent with the experimental value considering that the two values are not directly comparable. The mobility of lithium ions in the electrolyte is one order of magnitude less than that calculated in an aqueous system.[65]

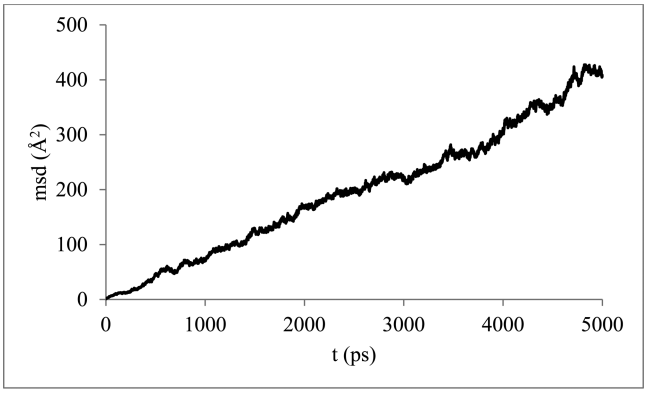

(a)

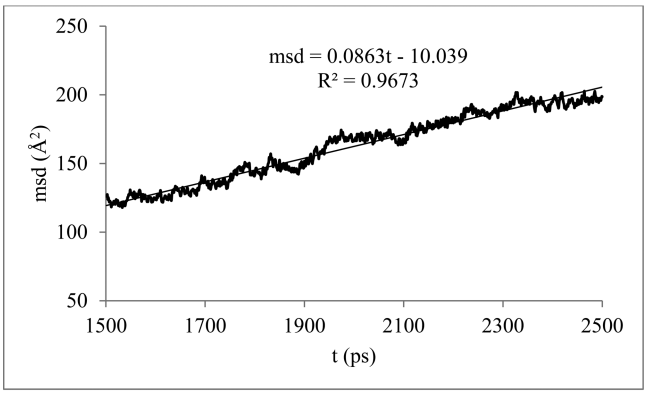

(b)

Figure 8. (a) Mean-square displacement as a function of time for the 1 M $LiPF_6$/EC mixture at 330 K in the *NVT* ensemble. (b) Diffusion coefficient (1.44×10^{-10} m^2/s) calculated as one-sixth of the slope in the linear region of the plot. The linear region was chosen where the correlation coefficient (R) was greater than 0.95.

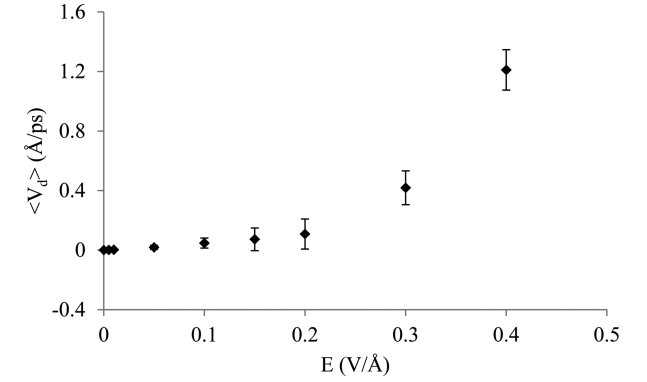

Figure 9. Drift velocity of Li^+ ions in EC under an external electric field. The deviations in drift velocity are due to the presence of different neighboring molecules around the cations, which can be present in both coupled ion pairs and solvent-separated ions.

4. CONCLUSIONS

We performed MD simulations and DFT calculations on a sample containing 1 M $LiPF_6$ in EC corresponding to a nanosize component of a battery. Such a nano arrangement is

DOI: 10.1021/acs.jpcc.6b03709
J. Phys. Chem. C 2016, 120, 16322−16332

an excellent test bed for determining properties and mechanisms. Both ab initio density functional theory analyses and classical molecular dynamics simulations showed that Li^+ ions are tetrahedrally coordinated to EC molecules. On the other hand, eight EC molecules surround each PF_6^- ion. Some of PF_6^- ions can enter the inner sphere of Li^+ ions solvated by EC molecules, as observed from the radial distribution plots. It is also very encouraging that the force field used is able to reproduce the characteristic features of pair distribution functions similar to those observed from electronic structure calculations. The melting and boiling points calculated using molecular dynamics simulations were within ±10 K of the experimental values. The diffusion coefficient of Li^+ ions in EC at 330 K was estimated to be 1.44×10^{-10} m^2/s, which is in close agreement with the experimental values of 1.82×10^{-10} m^2/s at 323 K and 2.33×10^{-10} m^2/s at 333 K.[61] The mobility, which is a good indicator of ion transport in the electrolyte, of Li^+ ions in EC calculated from the drift velocities was found to be in good agreement with related experiments. Therefore, by properly choosing the force field parameters in concert with DFT analyses, it will be possible to extend this type of analysis to other electrolytes to study ion mobility and thermodynamics and, eventually, to include electrodes to search for more powerful and more durable electrodes. Finally, as a side product of our trials to select a set of partial charges, we found that the use of Mulliken charges, despite their variation with different basis sets, is not worse than the use of NBO charges.

AUTHOR INFORMATION

Corresponding Author

*E-mail: seminario@tamu.edu. Tel.: 979-845-3301.

Notes

The authors declare no competing financial interest.

ACKNOWLEDGMENTS

We acknowledge the help of Victor Ponce and Diego E. Galvez-Aranda in the calculations of the molecular electrostatic potentials. We acknowledge funding from the Assistant Secretary for Energy Efficiency and Renewable Energy, Office of Vehicle Technologies, U.S. Department of Energy, under Contract DE-AC02-05CH11231, Subcontract 7060634 under the Advanced Batteries Materials Research (BMR) Program. We also appreciate the support of computational resources from Texas A&M High Performance Research Computing and the Texas Advanced Computing Center (TACC).

REFERENCES

(1) Soetens, J.-C.; Millot, C.; Maigret, B.; Bakó, I. Molecular Dynamics Simulation and X-ray Diffraction Studies of Ethylene Carbonate, Propylene Carbonate and Dimethyl Carbonate in Liquid Phase. *J. Mol. Liq.* **2001**, *92*, 201−216.

(2) Shi, S.; Lu, P.; Liu, Z.; Qi, Y.; Hector, L. G.; Li, H.; Harris, S. J. Direct Calculation of Li-Ion Transport in the Solid Electrolyte Interphase. *J. Am. Chem. Soc.* **2012**, *134*, 15476−15487.

(3) Yildirim, H.; Kinaci, A.; Chan, M. K. Y.; Greeley, J. P. First-Principles Analysis of Defect Thermodynamics and Ion Transport in Inorganic Sei Compounds: Lif and Naf. *ACS Appl. Mater. Interfaces* **2015**, *7*, 18985−18996.

(4) Ouyang, W.; Saven, J. G.; Subotnik, J. E. A Surface Hopping View of Electrochemistry: Non-Equilibrium Electronic Transport through an Ionic Solution with a Classical Master Equation. *J. Phys. Chem. C* **2015**, *119*, 20833−20844.

(5) Cao, Z.; Peng, Y.; Voth, G. A. Ion Transport through Ultrathin Electrolyte under Applied Voltages. *J. Phys. Chem. B* **2015**, *119*, 7516−7521.

(6) Takenaka, N.; Suzuki, Y.; Sakai, H.; Nagaoka, M. On Electrolyte-Dependent Formation of Solid Electrolyte Interphase Film in Lithium-Ion Batteries: Strong Sensitivity to Small Structural Difference of Electrolyte Molecules. *J. Phys. Chem. C* **2014**, *118*, 10874−10882.

(7) Aurbach, D.; Zinigrad, E.; Cohen, Y.; Teller, H. A Short Review of Failure Mechanisms of Lithium Metal and Lithiated Graphite Anodes in Liquid Electrolyte Solutions. *Solid State Ionics* **2002**, *148*, 405−416.

(8) Soto, F. A.; Ma, Y.; Martinez de la Hoz, J. M.; Seminario, J. M.; Balbuena, P. B. Formation and Growth Mechanisms of Solid-Electrolyte Interphase Layers in Rechargeable Batteries. *Chem. Mater.* **2015**, *27*, 7990−8000.

(9) Ma, Y.; Martinez de la Hoz, J. M.; Angarita, I.; Berrio-Sanchez, J. M.; Benitez, L.; Seminario, J. M.; Son, S.-B.; Lee, S.-H.; George, S. M.; Ban, C. M.; et al. Structure and Reactivity of Alucone-Coated Films on Si and Li_xsi_y Surfaces. *ACS Appl. Mater. Interfaces* **2015**, *7*, 11948−11955.

(10) Benitez, L.; Cristancho, D.; Seminario, J. M.; Martinez de la Hoz, J. M.; Balbuena, P. B. Electron Transfer through Solid-Electrolyte-Interphase Layers Formed on Si Anodes of Li-Ion Batteries. *Electrochim. Acta* **2014**, *140*, 250−257.

(11) Chen, Y. C.; Ouyang, C. Y.; Song, L. J.; Sun, Z. L. Electrical and Lithium Ion Dynamics in Three Main Components of Solid Electrolyte Interphase from Density Functional Theory Study. *J. Phys. Chem. C* **2011**, *115*, 7044−7049.

(12) Gauthier, M.; Carney, T. J.; Grimaud, A.; Giordano, L.; Pour, N.; Chang, H.-H.; Fenning, D. P.; Lux, S. F.; Paschos, O.; Bauer, C.; et al. Electrode−Electrolyte Interface in Li-Ion Batteries: Current Understanding and New Insights. *J. Phys. Chem. Lett.* **2015**, *6*, 4653−4672.

(13) Ouyang, W.; Saven, J. G.; Subotnik, J. E. A Surface Hopping View of Electrochemistry: Non-Equilibrium Electronic Transport through an Ionic Solution with a Classical Master Equation. *J. Phys. Chem. C* **2015**, *119*, 20833−20844.

(14) Cao, Z.; Peng, Y.; Voth, G. A. Ion Transport through Ultrathin Electrolyte under Applied Voltages. *J. Phys. Chem. B* **2015**, *119*, 7516−7521.

(15) Soetens, J.-C.; Millot, C.; Maigret, B.; Bakó, I. Molecular Dynamics Simulation and X-ray Diffraction Studies of Ethylene Carbonate, Propylene Carbonate and Dimethyl Carbonate in Liquid Phase. *J. Mol. Liq.* **2001**, *92*, 201−216.

(16) Freunberger, S. A.; Chen, Y.; Drewett, N. E.; Hardwick, L. J.; Bardé, F.; Bruce, P. G. The Lithium−Oxygen Battery with Ether-Based Electrolytes. *Angew. Chem., Int. Ed.* **2011**, *50*, 8609−8613.

(17) Leung, K.; Qi, Y.; Zavadil, K. R.; Jung, Y. S.; Dillon, A. C.; Cavanagh, A. S.; Lee, S.-H.; George, S. M. Using Atomic Layer Deposition to Hinder Solvent Decomposition in Lithium Ion Batteries: First-Principles Modeling and Experimental Studies. *J. Am. Chem. Soc.* **2011**, *133*, 14741−14754.

(18) Suo, L.; Borodin, O.; Gao, T.; Olguin, M.; Ho, J.; Fan, X.; Luo, C.; Wang, C.; Xu, K. "Water-in-Salt" Electrolyte Enables High-Voltage Aqueous Lithium-Ion Chemistries. *Science* **2015**, *350*, 938−943.

(19) Soetens, J.-C.; Millot, C.; Maigret, B. Molecular Dynamics Simulation of $Li^+BF_4^-$ in Ethylene Carbonate, Propylene Carbonate, and Dimethyl Carbonate Solvents. *J. Phys. Chem. A* **1998**, *102*, 1055−1061.

(20) Sambasivarao, S. V.; Acevedo, O. Development of OPLS-AA Force Field Parameters for 68 Unique Ionic Liquids. *J. Chem. Theory Comput.* **2009**, *5*, 1038−1050.

(21) Sun, H.; Mumby, S. J.; Maple, J. R.; Hagler, A. T. An ab Initio CFF93 All-Atom Force Field for Polycarbonates. *J. Am. Chem. Soc.* **1994**, *116*, 2978−2987.

(22) Cornell, W. D.; Cieplak, P.; Bayly, C. I.; Gould, I. R.; Merz, K. M.; Ferguson, D. M.; Spellmeyer, D. C.; Fox, T.; Caldwell, J. W.; Kollman, P. A. A Second Generation Force Field for the Simulation of

DOI: 10.1021/acs.jpcc.6b03709
J. Phys. Chem. C 2016, 120, 16322−16332

Proteins, Nucleic Acids, and Organic Molecules. *J. Am. Chem. Soc.* **1995**, *117*, 5179−5197.
(23) Masia, M.; Probst, M.; Rey, R. Ethylene Carbonate−Li^+: A Theoretical Study of Structural and Vibrational Properties in Gas and Liquid Phases. *J. Phys. Chem. B* **2004**, *108*, 2016−2027.
(24) Tasaki, K.; Harris, S. J. Computational Study on the Solubility of Lithium Salts Formed on Lithium Ion Battery Negative Electrode in Organic Solvents. *J. Phys. Chem. C* **2010**, *114*, 8076−8083.
(25) *Materials Studio 4.3*; Accelrys, Inc.: San Diego, CA, 2008.
(26) Wang, J.; Wolf, R. M.; Caldwell, J. W.; Kollman, P. A.; Case, D. A. Development and Testing of a General Amber Force Field. *J. Comput. Chem.* **2004**, *25*, 1157−1174.
(27) Jorn, R.; Kumar, R.; Abraham, D. P.; Voth, G. A. Atomistic Modeling of the Electrode−Electrolyte Interface in Li-Ion Energy Storage Systems: Electrolyte Structuring. *J. Phys. Chem. C* **2013**, *117*, 3747−3761.
(28) Borodin, O.; Smith, G. D. Development of Many-Body Polarizable Force Fields for Li-Battery Components: 1. Ether, Alkane, and Carbonate-Based Solvents. *J. Phys. Chem. B* **2006**, *110*, 6279−6292.
(29) Borodin, O. Polarizable Force Field Development and Molecular Dynamics Simulations of Ionic Liquids. *J. Phys. Chem. B* **2009**, *113*, 11463−11478.
(30) Vatamanu, J.; Borodin, O.; Smith, G. D. Molecular Dynamics Simulation Studies of the Structure of a Mixed Carbonate/$LiPF_6$ Electrolyte near Graphite Surface as a Function of Electrode Potential. *J. Phys. Chem. C* **2012**, *116*, 1114−1121.
(31) Borodin, O.; Zhuang, G. V.; Ross, P. N.; Xu, K. Molecular Dynamics Simulations and Experimental Study of Lithium Ion Transport in Dilithium Ethylene Dicarbonate. *J. Phys. Chem. C* **2013**, *117*, 7433−7444.
(32) Bedrov, D.; Smith, G. D.; van Duin, A. C. T. Reactions of Singly-Reduced Ethylene Carbonate in Lithium Battery Electrolytes: A Molecular Dynamics Simulation Study Using the ReaxFF. *J. Phys. Chem. A* **2012**, *116*, 2978−2985.
(33) Ong, M. T.; Verners, O.; Draeger, E. W.; van Duin, A. C. T.; Lordi, V.; Pask, J. E. Lithium Ion Solvation and Diffusion in Bulk Organic Electrolytes from First-Principles and Classical Reactive Molecular Dynamics. *J. Phys. Chem. B* **2015**, *119*, 1535−1545.
(34) Frisch, M. J.; Trucks, G. W.; Schlegel, H. B.; Scuseria, G. E.; Robb, M. A.; Cheeseman, J. R.; Scalmani, G.; Barone, V.; Mennucci, B.; Petersson, G. A.; Nakatsuji, H.; Caricato, M.; Li, X.; Hratchian, H. P.; Izmaylov, A. F.; Bloino, J.; Zheng, G.; Sonnenberg, J. L.; Hada, M.; Ehara, M.; Toyota, K.; Fukuda, R.; Hasegawa, J.; Ishida, M.; Nakajima, T.; Honda, Y.; Kitao, O.; Nakai, H.; Vreven, T.; Montgomery, J. A., Jr.; Peralta, J. E.; Ogliaro, F.; Bearpark, M.; Heyd, J. J.; Brothers, E.; Kudin, K. N.; Staroverov, V. N.; Keith, T.; Kobayashi, R.; Normand, J.; Raghavachari, K.; Rendell, A.; Burant, J. C.; Iyengar, S. S.; Tomasi, J.; Cossi, M.; Rega, N.; Millam, J. M.; Klene, M.; Knox, J. E.; Cross, J. B.; Bakken, V.; Adamo, C.; Jaramillo, J.; Gomperts, R.; Stratmann, R. E.; Yazyev, O.; Austin, A. J.; Cammi, R.; Pomelli, C.; Ochterski, J. W.; Martin, R. L.; Morokuma, K.; Zakrzewski, V. G.; Voth, G. A.; Salvador, P.; Dannenberg, J. J.; Dapprich, S.; Daniels, A. D.; Farkas, Ö.; Foresman, J. B.; Ortiz, J. V.; Cioslowski, J.; Fox, D. J. *Gaussian 09*, revision B.01; Gaussian Inc.: Wallingford, CT, 2010.
(35) Becke, A. D. Density Functional Thermochemistry. III. The Role of Exact Exchange. *J. Chem. Phys.* **1993**, *98*, 5648−5652.
(36) Perdew, J. P.; Burke, K.; Wang, Y. Generalized Gradient Approximation for the Exchange-Correlation Hole of a Many-Electron System. *Phys. Rev. B: Condens. Matter Mater. Phys.* **1996**, *54*, 16533.
(37) Perdew, J. P.; Chevary, J.; Vosko, S.; Jackson, K. A.; Pederson, M. R.; Singh, D.; Fiolhais, C. Atoms, Molecules, Solids, and Surfaces: Applications of the Generalized Gradient Approximation for Exchange and Correlation. *Phys. Rev. B: Condens. Matter Mater. Phys.* **1992**, *46*, 6671.
(38) Perdew, J. P.; Chevary, J.; Vosko, S.; Jackson, K. A.; Pederson, M. R.; Singh, D.; Fiolhais, C. Erratum: Atoms, Molecules, Solids, and Surfaces: Applications of the Generalized Gradient Approximation for Exchange and Correlation. *Phys. Rev. B: Condens. Matter Mater. Phys.* **1993**, *48*, 4978.
(39) Perdew, J. P., Ziesche, P., Eschrig, H., Eds. *Electronic Structure of Solids '91*; Akademie Verlag: Berlin, 1991; Vol. *11*.
(40) Francl, M. M.; Pietro, W. J.; Hehre, W. J.; Binkley, J. S.; Gordon, M. S.; DeFrees, D. J.; Pople, J. A. Self-Consistent Molecular Orbital Methods. XXIII. A Polarization-Type Basis Set for Second-Row Elements. *J. Chem. Phys.* **1982**, *77*, 3654−3665.
(41) Hehre, W. J.; Ditchfield, R.; Pople, J. A. Self-Consistent Molecular Orbital Methods. XII. Further Extensions of Gaussian-Type Basis Sets for Use in Molecular Orbital Studies of Organic Molecules. *J. Chem. Phys.* **1972**, *56*, 2257−2261.
(42) Plimpton, S. Fast Parallel Algorithms for Short-Range Molecular Dynamics. *J. Comput. Phys.* **1995**, *117*, 1−19.
(43) Bobadilla, A. D.; Seminario, J. M. Argon-Beam Induced Defects on Silica-Supported Single Walled Carbon Nanotube. *J. Phys. Chem. C* **2014**, *118*, 28299−28307.
(44) Bellido, E. P.; Seminario, J. M. Molecular Dynamics Simulations of Ion Bombarded Graphene. *J. Phys. Chem. C* **2012**, *116*, 4044−4049.
(45) Bobadilla, A. D.; Samuel, E. L. G.; Tour, J. M.; Seminario, J. M. Calculating the Hydrodynamic Volume of Poly(ethylene oxylated) Single-Walled Carbon Nanotubes and Hydrophilic Carbon Clusters. *J. Phys. Chem. B* **2013**, *117*, 343−354.
(46) Bobadilla, A. D.; Seminario, J. M. Assembly of a Noncovalent DNA Junction on Graphene Sheets and Electron Transport Characteristics. *J. Phys. Chem. C* **2013**, *117*, 26441−26453.
(47) Rodríguez-Jeangros, N.; Seminario, J. M. Density Functional Theory and Molecular Dynamics Study of the Uranyl Ion $(UO_2)^{2+}$. *J. Mol. Model.* **2014**, *20*, 2150.
(48) Bellido, E. P.; Seminario, J. M. Graphene Based Vibronic Devices. *J. Phys. Chem. C* **2012**, *116*, 8409−8416.
(49) Martínez, L.; Andrade, R.; Birgin, E. G.; Martínez, J. M. PACKMOL: A Package for Building Initial Configurations for Molecular Dynamics Simulations. *J. Comput. Chem.* **2009**, *30*, 2157−2164.
(50) Rappé, A. K.; Casewit, C. J.; Colwell, K.; Goddard, W., III; Skiff, W. UFF, a Full Periodic Table Force Field for Molecular Mechanics and Molecular Dynamics Simulations. *J. Am. Chem. Soc.* **1992**, *114*, 10024−10035.
(51) Rappe, A.; Colwell, K.; Casewit, C. Application of a Universal Force Field to Metal Complexes. *Inorg. Chem.* **1993**, *32*, 3438−3450.
(52) Humphrey, W.; Dalke, A.; Schulten, K. Vmd: Visual Molecular Dynamics. *J. Mol. Graphics* **1996**, *14*, 33−38.
(53) Dauber-Osguthorpe, P.; Roberts, V. A.; Osguthorpe, D. J.; Wolff, J.; Genest, M.; Hagler, A. T. Structure and Energetics of Ligand Binding to Proteins: Escherichia Coli Dihydrofolate Reductase-Trimethoprim, a Drug-Receptor System. *Proteins: Struct., Funct., Genet.* **1988**, *4*, 31−47.
(54) Sun, H. Compass: An Ab Initio Force-Field Optimized for Condensed-Phase Applicationsoverview with Details on Alkane and Benzene Compounds. *J. Phys. Chem. B* **1998**, *102*, 7338−7364.
(55) Canongia Lopes, J. N.; Pádua, A. A. H. Molecular Force Field for Ionic Liquids Composed of Triflate or Bistriflylimide Anions. *J. Phys. Chem. B* **2004**, *108*, 16893−16898.
(56) Shi, R.; Wang, Y. Ion-Cage Interpretation for the Structural and Dynamic Changes of Ionic Liquids under an External Electric Field. *J. Phys. Chem. B* **2013**, *117*, 5102−5112.
(57) Ren, G.; Shi, R.; Wang, Y. Structural, Dynamic, and Transport Properties of Concentrated Aqueous Sodium Chloride Solutions under an External Static Electric Field. *J. Phys. Chem. B* **2014**, *118*, 4404−4411.
(58) Collins, J. B.; Streitwieser, A. Integrated Spatial Electron Populations in Molecules: Application to Simple Molecules. *J. Comput. Chem.* **1980**, *1*, 81−87.
(59) Reed, A. E.; Weinstock, R. B.; Weinhold, F. Natural Population Analysis. *J. Chem. Phys.* **1985**, *83*, 735−746.
(60) Riddick, J. A.; Bunger, W. B.; Sakano, T. K. *Organic Solvents: Physical Properties and Methods of Purification*, 4th ed.; Techniques of Chemistry; John Wiley & Sons: New York, 1986; Vol. *2*.

DOI: 10.1021/acs.jpcc.6b03709
J. Phys. Chem. C 2016, 120, 16322−16332

(61) Hayamizu, K. Temperature Dependence of Self-Diffusion Coefficients of Ions and Solvents in Ethylene Carbonate, Propylene Carbonate, and Diethyl Carbonate Single Solutions and Ethylene Carbonate + Diethyl Carbonate Binary Solutions of $LiPF_6$ Studied by Nmr. *J. Chem. Eng. Data* **2012**, *57*, 2012−2017.
(62) Borodin, O.; Smith, G. D. Litfsi Structure and Transport in Ethylene Carbonate from Molecular Dynamics Simulations. *J. Phys. Chem. B* **2006**, *110*, 4971−4977.
(63) Kataoka, H.; Saito, Y.; Sakai, T.; Deki, S.; Ikeda, T. Ionic Mobility of Cation and Anion of Lithium Gel Electrolytes Measured by Pulsed Gradient Spin−Echo Nmr Technique under Direct Electric Field. *J. Phys. Chem. B* **2001**, *105*, 2546−2550.
(64) Saito, Y.; Kataok, H.; Deki, S. Ionic Mobility Measurements Applying a Controlled Direct Electric Field on Pulsed Gradient Spin Echo Nuclear Magnetic Resonance. *J. Electrochem. Soc.* **2001**, *148*, E382−E385.
(65) Lee, S. H.; Rasaiah, J. C. Molecular Dynamics Simulation of Ionic Mobility. I. Alkali Metal Cations in Water at 25 °C. *J. Chem. Phys.* **1994**, *101*, 6964−6974.

DOI: 10.1021/acs.jpcc.6b03709
J. Phys. Chem. C 2016, 120, 16322−16332